

Article

# Investigation of Platinum-Group Minerals (PGM) from Othrys Chromitites (Greece) Using Superpanning Concentrates

Basilios Tsikouras <sup>1,2,\*</sup>, Elena Ifandi <sup>2</sup>, Sofia Karipi <sup>2</sup>, Tassos A. Grammatikopoulos <sup>3</sup> and Konstantin Hatzipanagiotou <sup>2</sup>

<sup>1</sup> Faculty of Science, Physical and Geological Sciences, Jalan Tungku Link, Universiti Brunei Darussalam, Gadong, BE1410, Brunei Darussalam

<sup>2</sup> Department of Geology, Section of Earth Materials, University of Patras, 26500 Patras, Greece; selena.21@windowslive.com (E.I.); skaripi@upatras.gr (S.K.); k.hatzipanagiotou@upatras.gr (K.H.)

<sup>3</sup> SGS Canada Inc., 185 Concession Street, PO 4300, Lakefield, ON K0L 2H0, Canada; tassos.grammatikopoulos@sgs.com

\* Correspondence: basilios.tsikouras@ubd.edu.bn; Tel.: +673-246-3001 (ext. 1682)

Academic Editor: Federica Zaccarini

Received: 7 June 2016; Accepted: 30 August 2016; Published: 12 September 2016

**Abstract:** Platinum-group minerals were concentrated using superpanning from two composite chromitite samples, which were collected from two old mines within the Othrys ophiolite. This method allows for the recovery of a broad spectrum of these rare and fine-grained minerals, and helps to better identify them and interpret their origin. Major differences between the east and west Othrys ophiolites were determined, probably as a result of their different origin and evolution. Primary Os-, Ir-, and Ru-bearing platinum-group minerals (IPGM)-alloys and the Rh-, Pt- and Pd-bearing platinum-group minerals (PPGM) occur only in the east Othrys chromitite, indicating an evolution from initially low  $f_{S_2}$  conditions at shallower mantle levels with the subsequent implication of a S-saturated ascending fluid. In contrast, the absence of primary IPGM-alloys in west Othrys chromitite indicates that S saturation had been attained. The presence of erlichmanite suggests that sulphur fugacity eventually increased significantly in both suites. Substantial fluctuations of a fluid phase, likely related to serpentinising fluids, modified the platinum-group minerals (PGM) assemblage of west Othrys, and resulted in a large diversity of secondary PGM minerals. The limited number of secondary species developed in the east Othrys indicate that secondary processes were also different in the two suites.

**Keywords:** PGM; IPGE; PPGE; Othrys ophiolite; chromitite; Greece

## 1. Introduction

Chromitites are one of the major primary host lithologies of platinum-group elements (PGE) and one of the main targets for their exploration [1–5]. Theoretical and experimental results suggest that silicate minerals (e.g., olivine, and pyroxenes) do not significantly contribute to the Ir- and Pd-groups PGE (IPGE: Os, Ir, and Ru; and PPGE: Rh, Pt, and Pd) budget of mantle rocks, despite the fact that they clearly dominate the upper mantle formations (e.g., [6,7]). Platinum-group minerals (PGM) comprise a crucial control factor on the budget of PGE in chromitites ([8] and references therein). Moreover, and besides their economic importance, the distribution of PGM in chromitites and the associated ultramafic rocks provide an important petrological window to the evolution of the mantle source from which they are derived. Different types of PGM control the distribution and bulk concentration of the PGE in their host formations [9,10]. The unique behaviour of PGE may provide significant insights into the crystallisation history and evolution of their mantle sources. PGE comprise also

significant petrogenetic indicators, as they remain largely unaffected from geochemical processes that fractionate and modify the lithophile elements in silicate and non-silicate rocks [4,11,12]. Despite the fact that ophiolitic chromitites are generally poorer in PGE than layered intrusions (e.g., [8]), their study can provide evidence for the understanding of mantle processes and the geodynamic evolution of the oceanic lithosphere, yet comprising important carriers of PGM. In the last decades, numerous experimental and empirical studies have provided data from PGM. However, their exact mechanism of formation and the details of their links to chromites are still debated (for a review see [8]). It has been proposed that PGM may form: (i) by direct precipitation from melts before the formation of chromites; (ii) by the breakdown of pre-existing PGE phases, which were incorporated in the parental melt of chromites; (iii) by precipitation from infiltrating fluids in chromitites that were transported deeper in the mantle by subduction; and (iv) by subsolidus recrystallisation.

In most of the studied ophiolitic chromitites worldwide, laurite ( $\text{RuS}_2$ ) constitutes the most abundant PGM phase followed by erlichmanite ( $\text{OsS}_2$ ). Both minerals can form extensive solid solutions, containing Ir as well, and mainly account for the Ru–Os–Ir dominated composition of their hosts. Most research on PGM relies exclusively on in situ observations in natural chromitite samples, which provides information and interpretations based on small size ( $<30 \mu\text{m}$ ) and sporadic mineral grains, which are not representative of the rocks. Although such studies are important in obtaining petrogenetic information, they frequently fail to properly assess several microscopic PGM phases and their statistical variance. On the contrary, initial processing of the host samples has been used to provide quantitative mineralogical data of the PGM in concentrates, using a variety of techniques. However, it should be noted that most of the in situ textural details between the PGM and their hosts are lost during the concentration processes, due to crushing, unless the PGM remain attached to or locked into the host. Therefore, caution is needed when these results are used for petrological interpretations. The investigation of concentrates has been used as a supplementary method to in situ investigation, to further understand the formation of PGM and the evolution of the Earth's mantle [13–15].

To our knowledge, there is only one description of PGM in the Othrys ophiolite reporting mainly the presence of laurite-erlichmanite series minerals, from both west and east Othrys [16]. According to this study the PGM are present as sulphides ( $<15 \mu\text{m}$ ) and are closely associated with chromite, enstatite, Na-rich pargasite, clinopyroxene, phlogopite, and Cu–Ni sulphides. Laurite often has an Os-rich composition. The highest Os concentrations in laurite are observed in a chromitite from Tsangli (east Othrys). The mainly euhedral shape and other textural and compositional features suggest that the Othrys PGM are of primary origin and may indicate an evolution from an early magmatic crystallisation.

The current study focuses on the recovery of a large number of PGM from composite samples and comprises a more detailed description of the minerals from both the west and east Othrys chromitites. A large variety of PGM is demonstrated in these ophiolitic chromitites, which are characterised by low PGE grades. Based on these PGM assemblages, we also attempt to contribute to the petrogenetic evolution of the Othrys ophiolite.

## 2. Materials and Methods

Approximately 20 kg of chromitite were collected from each of two abandoned mines in Tsangli and Agios Stefanos, occurring at the NE and SW parts of the Othrys ophiolite complex, respectively. Fresh samples were collected from the internal parts of natural chromitite exposures and away from the ore margins. Subsequently, they were crushed, blended and homogenised to generate a composite sample from each area. Following initial homogenisation, approximately 1 kg of material from each composite sample was further comminuted to produce about 800 g of material in the grain size of  $<75 \mu\text{m}$ . This material was subjected to heavy liquid separation technique (density of heavy liquids =  $2.9 \text{ g/cm}^3$ ) to produce heavy- and light-mineral concentrates. The former was mainly dominated by chromite, sulphides and PGM, while the latter mostly included silicate minerals.

A previous study reported that the grain size of PGM hosted in the Othrys chromitites is less than 15  $\mu\text{m}$  in diameter [16].

In the present study, the heavy-mineral concentrate was further divided into two size fractions of <38  $\mu\text{m}$  (−400 mesh) and >38  $\mu\text{m}$  (+400 mesh) in order to investigate the PGM. Each of the two size fractions was subjected to a superpanning technique to produce three different fractions, tip, chromite and tail, of different density (for a detailed description of the method see [17]). The tip and chromite fractions were the densest particles, mostly including liberated grains of PGM and chromite, relative to the lighter tail fraction, which was mostly dominated by silicates. One polished section was prepared from each tip and chromite fractions, for each of the size fractions and from each composite sample. The concentrates were initially screened and the PGM were microanalysed using a JEOL JSM-6300 (Peabody, MA, USA) scanning electron microscope (SEM) equipped with energy dispersive spectrometer (EDS) and wavelength dispersive spectrometer (WDS), at the Laboratory of Electron Microscopy and Microanalysis at the University of Patras, Greece (operating conditions: accelerating voltage 20 kV, beam current 3 nA).

Backscattered electron images (BSEI) were processed and semi-automatic counts and surface measurements of all the PGM grains were elaborated with image analysis techniques using the Leica Q-Win (Leica Microsystems, Wetzlar, Germany) and JMicroVision v.1.2.7 software. The equivalent circular diameter (ECD = two times the square root of the area over  $\pi$ ) was calculated from the surface measurements. It is critical to note that these analyses are used to identify the PGM and not to quantify their chemistry. Furthermore, analysis of fine-grained PGM is always tentative. Selected BSEI were processed using the pseudocolourisation mode of JMicroVision v.1.2.7 software (image operation: Image Factory/Operation/Pseudocolour/Spectrum) in order to reveal and enhance the textural characteristics and the compositional inhomogeneities of the crystals. This operation uses pseudocolours on an image replacing the standard lookup table that defines the original colour of a pixel with a range of specified colour palettes listed in the software library. Thus, the original characteristics of the mineral phases, in each image, remain the same but they are represented with different colours. These pseudocolours highlight compositional differences and textural features in a crystal or crystal aggregates, as they are derived from different shades of grey. Different contrast and hues of grey in different images, even for the same mineral, result in variable pseudocolourisation. Therefore, this operation provides conclusive pictures in each individual image and must not be used for comparisons between images.

### 3. Geological Setting

The Othrys ophiolite outcrops in eastern central Greece (Figure 1). It is part of the west ophiolitic belt of Greece that extends in a NW-SE direction and includes the ophiolitic sequences of Vourinos and Pindos, as well as the Albanides and Dinarides to the north. This ophiolite belt represents a suture from closing of the Mesozoic Tethys oceanic crust and contains the podiform chromite ore deposits of Pindos, Vourinos and Othrys in Greece, as well as of the Tropoja and Bulqiza in Albania (e.g., [13–15,18,19]).

The Othrys ophiolite comprises a dismembered complex divided in two main bodies: a western and an eastern one. It includes an uppermost nappe pile where the ophiolitic rocks are dismembered and emplaced in reverse stratigraphic order (Figure 2). These ophiolitic rocks form part of a series of thrusts, known as the Mirna Group, which reveal lateral transition from continental material (clastic sediments and shallow water carbonates) to pelagic carbonates of the Mesozoic Pelagonian Zone [20,21]. The Sipetorrema Pillow Lava unit (after [20]) comprises the lowermost structural ophiolite member and includes pillow lavas, rare lava flows and interbedded siltstone and chert. It is structurally overlain by the Kournovon Dolerite unit (approximately 150 m thick), which is comprised of vertical sheeted dolerite penetrating minor cumulate gabbro. The higher structural members comprise dismembered oceanic mantle rocks dominated by medium- to coarse-grained, variably serpentinised harzburgite with minor lherzolite, plagioclase lherzolite and dunite (e.g., [22–25]). Chromitite deposits occur in two

major parts of the Othrys complex. They are hosted in two tectonically separated ultramafic bodies, at the regions of Domokos (west Othrys ophiolite) and Eretria (east Othrys ophiolite). The Metalleion and Agios Stefanos chromitite mines outcrop in the west Othrys, whereas the Tsangli and Kastraki occur in the east Othrys ophiolite (Figure 2). Samples for this study were collected from Agios Stefanos and the Tsangli mines, both including predominantly massive chromitites, occurring as podiform, lenticular or irregular ore bodies, randomly distributed in highly serpentinised dunite within harzburgite [16].

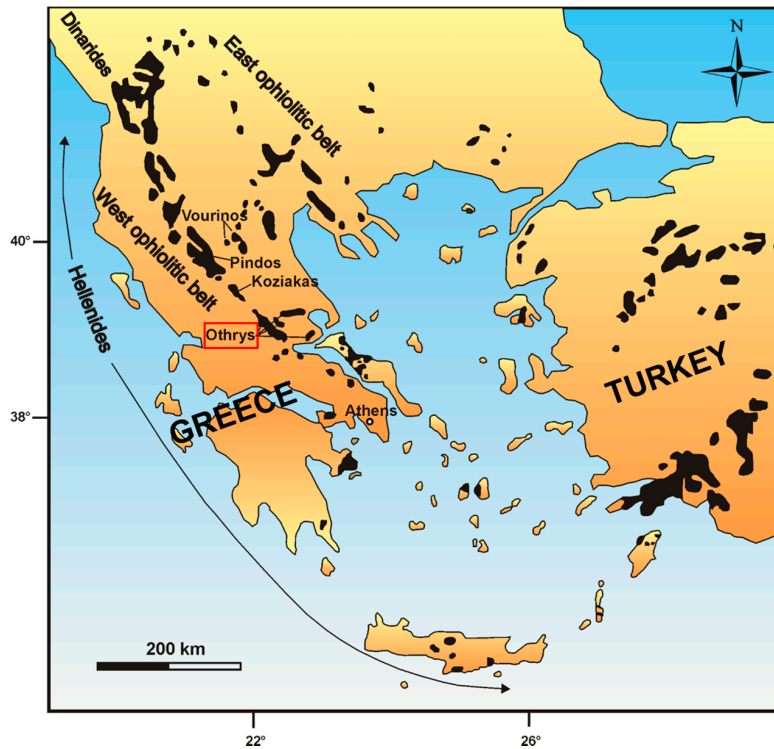


Figure 1. Distribution of the two ophiolitic belts in Greece and west part of Turkey (modified after [26]).

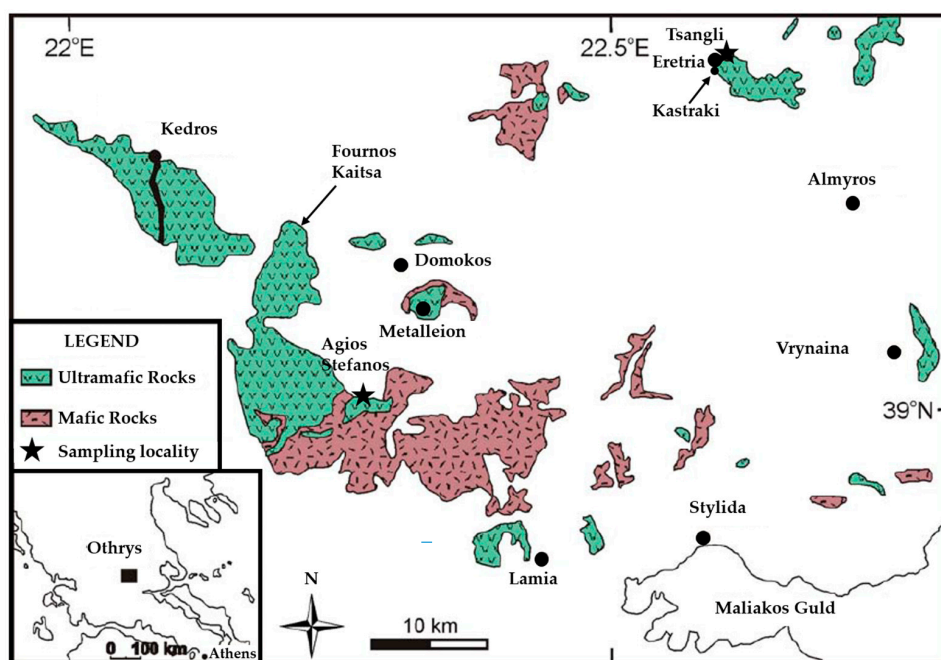


Figure 2. Simplified geological map of the Othrys ophiolite (modified after [23]).

### 4. PGM Distribution

#### 4.1. Agios Stefanos Sample

##### 4.1.1. Tip Fraction (−400 Mesh)

Details for the type and the surface area of PGM from the Agios Stefanos fractions are listed in Table 1. Statistical processing of mineral distribution and grain size are comparatively illustrated in Figures 3 and 4. Representative BSEI of PGM are shown in Figure 5. The modal abundance of the PGM assemblage was calculated on the basis of the surface area of the minerals. This finer-grained tip includes erlichmanite (40.43%), laurite (38.25%), mixed phases (10.47%), IPGE–Ni alloys (mostly Ru–Os–Ir–Ni alloys) (3.38%), laurite-erlichmanite solid solution (3.15%), desulphurised laurite and/or erlichmanite (2.09%), and Ag–Pd alloys (1.22%). Minor amounts of irarsite (0.79%), native Ag (0.16%), Pt–Cu alloys (0.04%), Os–Ir–Pt alloys (0.01%) and irarsite-osarsite (0.004%) were also observed (Figures 3a and 5a–f). Mixed phases include composite grains of complex intergrowths of Pd–Sb–Cu alloys, Pd–Cu–Pt alloys, cooperite, as well as desulphurised irarsite, platarsite, irarsite-platarsite, hollingworthite, and cooperite-braggite. The identification of these phases was qualitative due to their small grain size. On the basis of the number of grains, this tip is dominated by erlichmanite (34.45%) and laurite (28.57%) followed by desulphurised laurite and/or erlichmanite (10.92%), mixed phases (9.24%), IPGE–Ni alloys (5.88%), laurite-erlichmanite (4.20%), irarsite (2.52%) and equal percentages of Os–Ir–Pt alloys, Pt–Cu alloys, Ag, Ag–Pd alloys and irarsite-osarsite (0.84% each; Figure 3a).

The grain size distribution indicates that the majority of the grains (93% or 78.8% by frequency) are up to 15 μm, 25 of which (21.2%) are less than 5 μm. Twenty-five grains (21.2%) are larger than 15 μm, two of which (one laurite and one erlichmanite) fall in the range of 25–35 μm (Figure 4a).

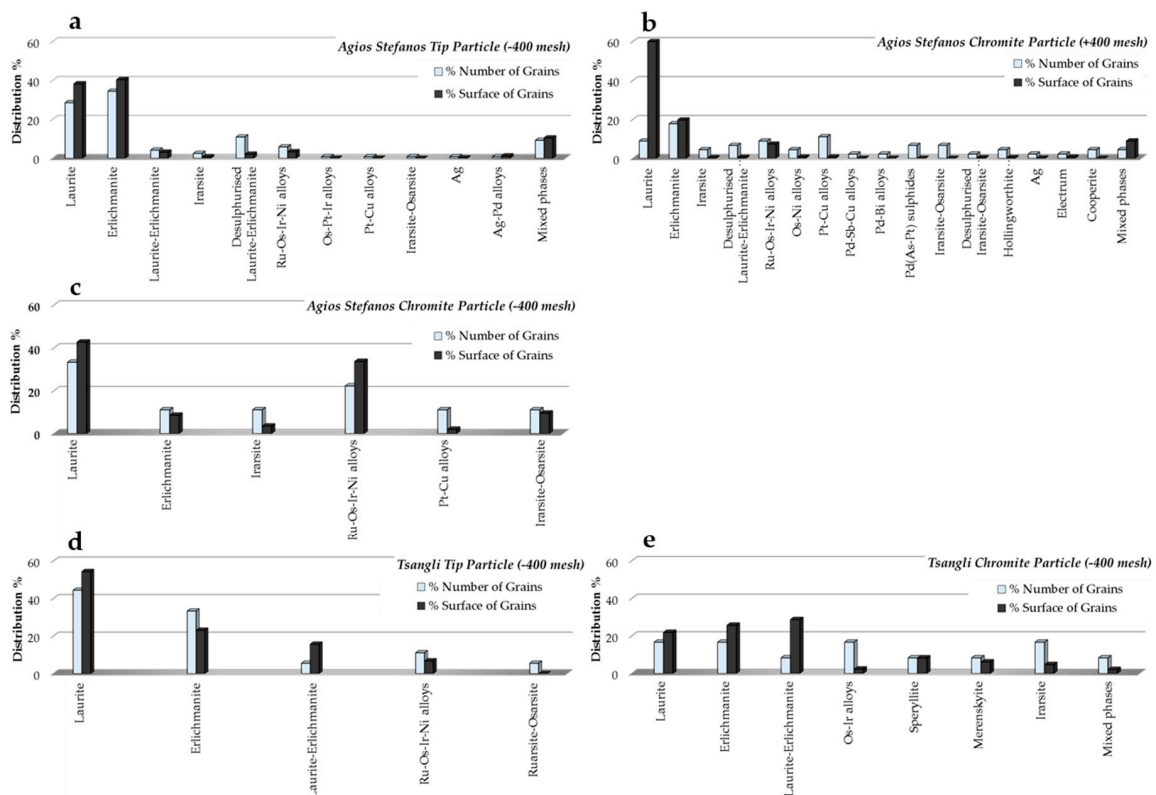


**Figure 3.** Plot of the statistical data of PGM distribution according to their number of grains and surface area from the: Agios Stefanos (a–c); and Tsangli (d,e) samples.

**Table 1.** Statistical data for the PGM grains from Agios Stefanos and Tsangli chromitite mines, Othrys.

Minerals	Agios Stefanos										Tsangli									
	Tip (−400 mesh)				Tip (+400 mesh)				Chromite (−400 mesh)				Tip (−400 mesh)				Chromite (−400 mesh)			
	Grains		Area		Grains		Area		Grains		Area		Grains		Area		Grains		Area	
	Number	%	Total um <sup>2</sup>	%	Number	%	Total um <sup>2</sup>	%	Number	%	Total um <sup>2</sup>	%	Number	%	Total um <sup>2</sup>	%	Number	%	Total um <sup>2</sup>	%
Laurite	34	28.57	5475.1	38.25	4	8.89	1684.9	59.96	3	33.33	108.5	42.70	8	44.44	1323.0	54.37	2	16.67	117.7	21.89
Erlichmanite	41	34.45	5787.0	40.43	8	17.78	20.1	19.71	1	11.11	21.7	8.54	6	33.33	561.9	23.09	2	16.67	138.0	25.66
Laurite-Erlichmanite	5	4.20	451.4	3.15	-	-	-	-	1	5.56	381.8	15.69	1	8.33	154.3	28.69	2	16.67	12.8	2.38
Os-Ir alloys	-	-	-	-	-	-	-	-	-	-	-	-	-	-	-	-	1	8.33	44.7	8.31
Speryllite	-	-	-	-	-	-	-	-	-	-	-	-	-	-	-	-	-	-	-	-
Desulphurised Laurite	7	5.88	57.4	0.40	1	2.22	5125.0	0.06	-	-	-	-	-	-	-	-	-	-	-	-
Desulphurised Erlichmanite	5	4.20	223.3	1.56	1	2.22	4.8	0.24	-	-	-	-	-	-	-	-	-	-	-	-
Desulphurised Laurite-Erlichmanite	1	0.84	18.5	0.13	1	2.22	21.3	0.25	-	-	-	-	-	-	-	-	-	-	-	-
Ru-Os-Ir-Ni alloys	7	5.88	484.2	3.38	4	8.89	624.6	7.31	2	22.22	85.6	33.69	2	11.11	166.0	6.82	-	-	-	-
Os-Ni alloys	-	-	-	-	2	4.44	57.7	0.68	-	-	-	-	-	-	-	-	-	-	-	-
Irasite	3	2.52	112.7	0.79	2	4.44	28.9	0.34	1	11.11	8.9	3.50	-	-	-	-	2	16.67	25.6	4.76
Irasite-Osarsite	1	0.84	0.6	0.00	3	6.67	2.9	0.03	1	11.11	24.3	9.56	-	-	-	-	-	-	-	-
Ruarsite-Osarsite	-	-	-	-	-	-	-	-	-	-	-	-	1	5.56	0.6	0.02	-	-	-	-
Desulphurised Irasite-Osarsite	-	-	-	-	1	2.22	30.2	0.35	-	-	-	-	-	-	-	-	-	-	-	-
Pt-Cu alloys	1	0.84	5.5	0.04	5	11.11	60.8	0.71	1	11.11	5.1	2.01	-	-	-	-	-	-	-	-
Os-Ir-Pt alloys	1	0.84	1.3	0.01	-	-	-	-	-	-	-	-	-	-	-	-	-	-	-	-
Pd-Sb-Cu alloys	-	-	-	-	1	2.22	4.6	0.05	-	-	-	-	-	-	-	-	-	-	-	-
Pd-Bi alloys	-	-	-	-	1	2.22	9.2	0.11	-	-	-	-	-	-	-	-	-	-	-	-
Hollingworthite	-	-	-	-	2	4.44	32.1	0.38	-	-	-	-	-	-	-	-	-	-	-	-
Cooperite	-	-	-	-	2	4.44	1.6	0.02	-	-	-	-	-	-	-	-	-	-	-	-
Pd(As-Pt) sulphides	-	-	-	-	3	6.67	2.6	0.03	-	-	-	-	-	-	-	-	-	-	-	-
Merenskyite	-	-	-	-	-	-	-	-	-	-	-	-	-	-	-	-	1	8.33	33.2	6.17
Ag	1	0.84	23.0	0.16	1	2.22	13.8	0.16	-	-	-	-	-	-	-	-	-	-	-	-
Ag-Pd alloys	1	0.84	175.0	1.22	-	-	-	-	-	-	-	-	-	-	-	-	-	-	-	-
Electrum	-	-	-	-	1	2.22	57.1	0.67	-	-	-	-	-	-	-	-	-	-	-	-
Mixed phases	11	9.24	1499.3	10.47	2	4.44	765.0	8.95	-	-	-	-	-	-	-	-	1	8.33	11.5	2.14

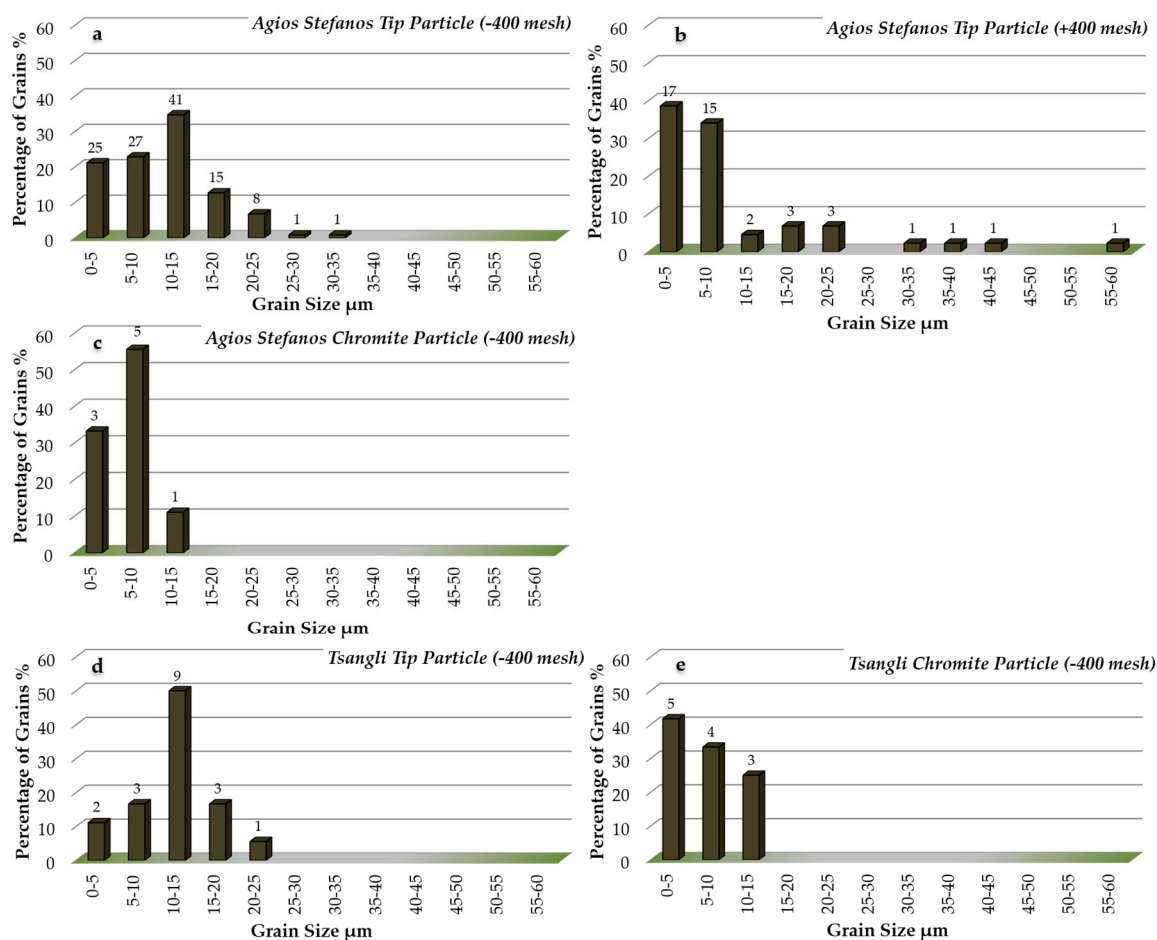


**Figure 4.** Plot of the statistical data of PGM grain sizes (ECD) from the: Agios Stefanos (a–c) and Tsangli (d,e) samples. Number of grains are indicated on top of the bars.

#### 4.1.2. Tip Fraction (+400 Mesh)

On the basis of surface area, laurite is the dominant PGM (59.96%) in this coarser-grained tip followed by lesser erlichmanite (19.71%), mixed phases (8.95%) and IPGE–Ni alloys (7.31%). Minor amounts of Pt–Cu alloys (0.71%), Os–Ni alloys (0.68%), electrum (0.67%), desulphurised laurite and/or erlichmanite (0.54%), irarsite-hollingworthite (0.38%), desulphurised irarsite-osarsite (0.35%), irarsite (0.34%), native Ag (0.16%), Pd–Bi alloys (0.11%), Pd–Sb–Cu alloys (0.05%), irarsite-osarsite (0.03%), Pd(As–Pt) sulphides (0.03%) and cooperite (0.02%) are also present (Table 1, Figures 3b and 5g–h). Mixed phases include complex intergrowths of a variety of alloys, sulphides and desulphurised phases. Based on the number of grains, the tip contains erlichmanite (17.78%), Pt–Cu alloys (11.11%), laurite (8.89%), and IPGE–Ni alloys (8.89%); equal amounts of desulphurised laurite-erlichmanite, irarsite-osarsite and Pd(As–Pt) sulphides (6.67% each); equal amounts of Os–Ni alloys, irarsite, irarsite-hollingworthite, and cooperite and mixed phases (4.44% each); and equal amounts of Pd–Sb–Cu alloys, Pd–Bi alloys, native Ag, electrum and desulphurised irarsite-osarsite (2.22% each; Figure 3b).

Most of the grains (32) representing 72.7% by frequency are smaller than 10 μm, whereas eight grains (18.2%) have a diameter between 10 and 25 μm. Three distinctively larger grains (6.9%) range between 30 and 45 μm including one erlichmanite (31.6 μm) and two laurites (36.4–40.6 μm). One laurite grain has an ECD of 56.7 μm and it is binned in the 55–60 μm class (Figure 4b).

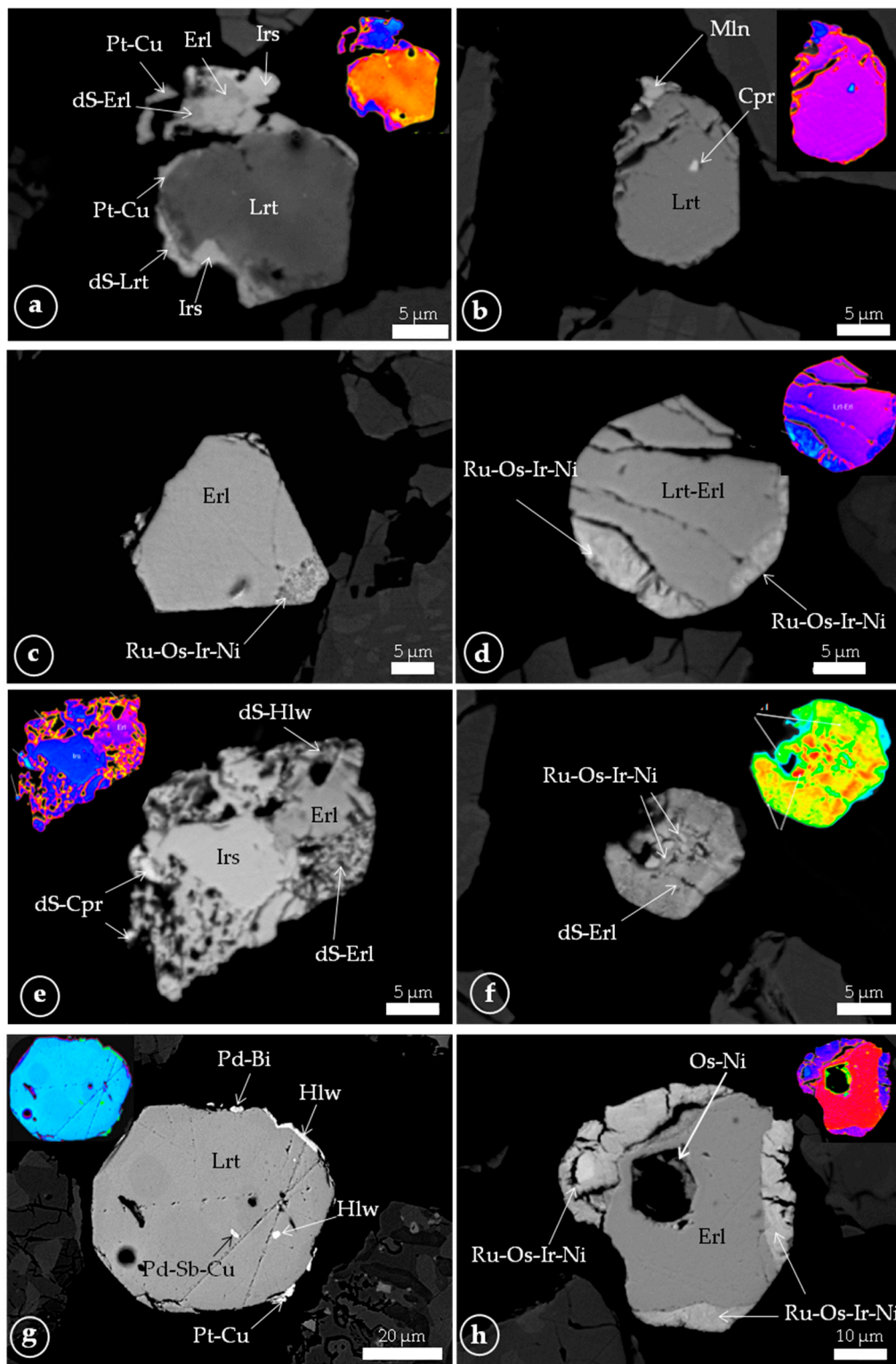


**Figure 5.** Backscattered electron images combined with their pseudocolourised images (insets) of PGM from the Agios Stefanos composite sample: (a–f) fine tip fraction (–400 mesh); and (g,h) coarse tip fraction (+400 mesh). Mineral abbreviations are: Cpr: cooperate; Erl: erlichmanite; Hlw: hollingworthite; Irs: irarsite; Lrt: laurite; Lrt-Erl: laurite-erlichmanite solid solution; Mln: malanite; and dS: desulphurised. For details, see text.

#### 4.1.3. Chromite Fraction (−400 Mesh)

The prevailing minerals by surface include laurite (42.70%), IPGE–Ni alloys (33.69%), irarsite-osarsite (9.56%), erlichmanite (8.54%), irarsite (3.50%) and Pt–Cu alloys (2.01%) (Table 1, Figure 3c). A calculation based on the number of grains indicate the predominance of laurite (33.33%) followed by IPGE–Ni alloys (22.22%), while each of erlichmanite, irarsite, irarsite-osarsite and Pt–Cu alloys are represented by one grain (11.11%) (Figure 3c).

Five out of the nine grains (55.6% by frequency) have an ECD between 5 and 10  $\mu\text{m}$ , three grains (33.3%) are less than 5  $\mu\text{m}$ , and one grain of an IPGE–Ni alloy (11.1%) is found in the range of 10–15  $\mu\text{m}$  (Figure 4c). The coarse fraction of chromite (+400 mesh) was PGM-free.

#### 4.2. Tsangli Sample

##### 4.2.1. Tip Fraction (−400 Mesh)

Results for the grain size and PGM types from the Tsangli fractions are listed in Table 1 and their statistical calculations are graphically illustrated in Figures 3 and 4. Representative BSEI of PGM are shown in Figure 6. Surface area measurements revealed the predominance of laurite (54.37%), followed by erlichmanite (23.09%), laurite–erlichmanite solid solution (15.69%) IPGE–Ni alloys (6.82%), and ruarsite–osarsite solid solution (0.02%; Figures 3d and 6a). On the basis of the number of grains, laurite (44.44%) and erlichmanite (33.33%) are the dominant PGM, followed by IPGE–Ni alloys (11.11%) and equally distributed grains (5.56% each) of laurite–erlichmanite, and ruarsite–osarsite solid solutions (Figure 3d).

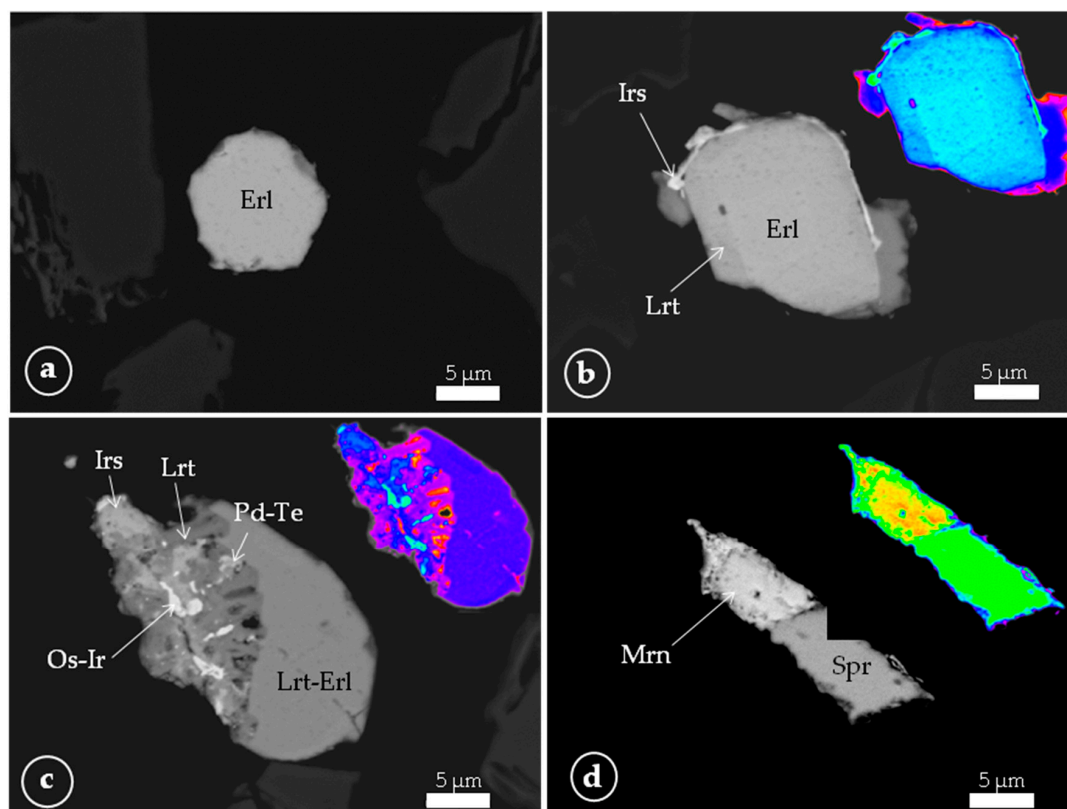


**Figure 6.** Backscattered electron images combined with their pseudocolourised images (insets) of PGM from the Tsangli composite sample: (a) fine tip fraction (−400 mesh); and (b–d) chromite fraction (−400 mesh). Mineral abbreviations are: Erl: erlichmanite; Irs: irarsite; Lrt: laurite; Lrt–Erl: laurite–erlichmanite solid solution; Mrn: merenskyite; and Spr: sperrylite. See text for details.

Half of the grains (9) have a size between 10 and 15  $\mu\text{m}$ , five grains (27.8% by frequency) are smaller than 10  $\mu\text{m}$ , three grains (16.7%) range between 15 and 20  $\mu\text{m}$ , and only one grain (5.6%) of laurite-erlichmanite with an ECD of 22  $\mu\text{m}$  is binned in the range of 20–25  $\mu\text{m}$  (Figure 4d).

#### 4.2.2. Tip Fraction (+400 Mesh)

The tip (+400 mesh) contains only one grain of laurite, which is classified in the 15–20  $\mu\text{m}$  bin size.

#### 4.2.3. Chromite Fraction (−400 Mesh)

On the basis of surface area, laurite-erlichmanite solid solution (28.69%), erlichmanite (25.66) and laurite (21.89%) are the prevailing PGM in this fraction (Figures 3e and 6b–c). Sperrylite (8.31%), merenskyite (6.17%), irarsite (4.76%), Os–Ir alloys (2.38%) and mixed phases (2.14%) are also present (Figures 3e and 6d). Mixed phases include complex intergrowths of irarsite and Os–Ir alloys. Two grains each of laurite, erlichmanite, irarsite and Os–Ir alloys (16.67% each), and one grain each of laurite-erlichmanite, sperrylite, merenskyite, and mixed phases (8.33% each) occur in this sample.

The vast majority of the grains (9% or 75.0% by frequency) are smaller than 10  $\mu\text{m}$ , whereas three grains (25.0%) (an erlichmanite, a laurite and a laurite-erlichmanite) are binned in the 10–15  $\mu\text{m}$  class (Figure 4e). The coarse fraction of chromite (+400 mesh) was PGM-free.

## 5. Mineralogical Characterisation of PGM

PGM from both the Agios Stefanos and Tsangli concentrates include primary, as well as secondary assemblages (Figure 7). The primary minerals observed in Agios Stefanos show mainly euhedral-subhedral or polygonal and lesser anhedral grains, while the primary PGM grains from Tsangli show generally a more irregular habit. In contrast, PGM with rounded boundaries, rugged surfaces, porous internal structures, replacive blebs or zoning (i.e., due to possibly progressive loss of S) are indicative of their secondary origin. These last crystals commonly replace primary phases or less frequently occur as independent grains.

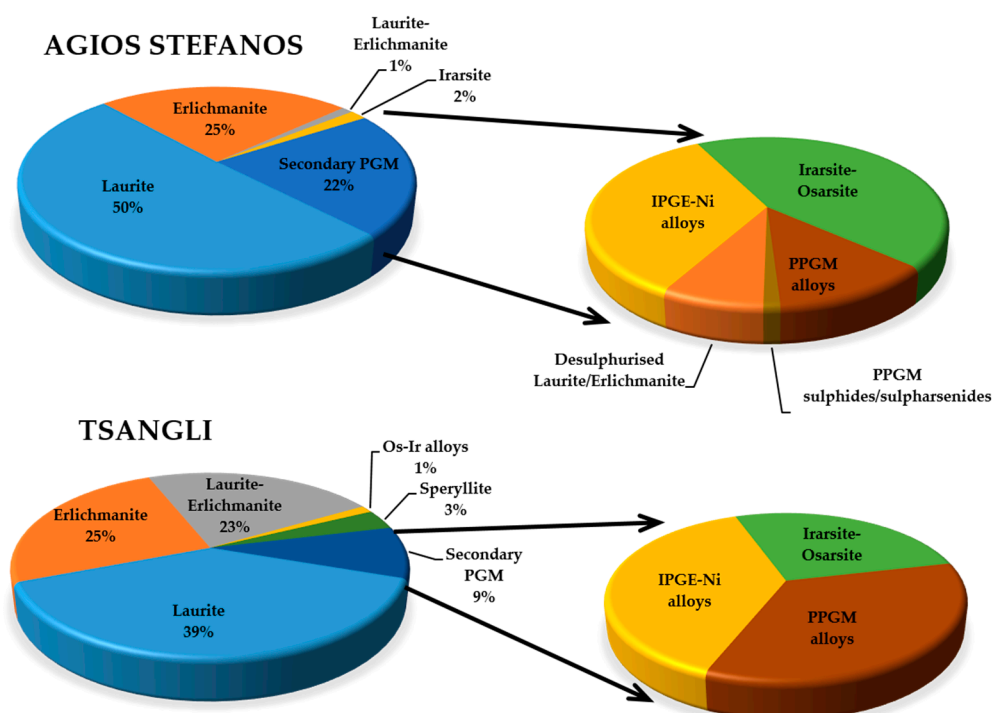


**Figure 7.** Pie charts of the collective modal abundance of PGM groups (primary and secondary assemblages) in all fractions from Agios Stefanos and Tsangli.

The Agios Stefanos sample shows a greater diversity of PGM relative to Tsangli (Figure 3). The primary PGM assemblage comprises mainly IPGE-phases including laurite, erlichmanite, and few laurite-erlichmanite (showing extensive solid solution) and scarce irarsite-osarsite (Figures 5 and 7). Erlichmanite occurs as subhedral to euhedral crystals in the tips, whereas laurite is comprised of fewer but generally larger grains, as it is deduced by its total larger surface area (Figure 3a–c). Large, subhedral to anhedral laurite prevails in the PGM grains that remained in the chromite fraction. Erlichmanite and irarsite-osarsite are less and smaller relative to the laurite in this fraction. Primary PPGE minerals are virtually absent in the Agios Stefanos sample. The Tsangli sample includes fewer species and a smaller number of grains of PGM (Figure 3). Primary, subhedral (rarely euhedral) laurite, erlichmanite and lesser laurite-erlichmanite grains were found in both the fine tip and chromite fractions (Figures 6a–c and 7). Rarely, grains of Os–Ir alloys, which are Ni-free, occur as inclusions in laurite, hence they are interpreted as early primary crystals (Figure 6c). A composite grain of sperrylite and merenskyite indicates that the first is a primary phase, whereas the associated sieved-textured merenskyite is secondary after sperrylite. (Figure 6d). No other significant differences are observed between the PGM grains occurring in the tip and chromite fraction from Tsangli.

Secondary PGM are similar in both tip fractions of the Agios Stefanos sample. Desulphurised erlichmanite typically occurs at the rims of primary crystals, whereas rare hollingworthite and irarsite-osarsite, as well as replacive IPGE–Ni alloys occur after erlichmanite and laurite (Figures 5a,c–h and 7). The replacive IPGE–Ni grains are commonly associated with desulphurised phases, and constitute evidence of their secondary origin (Figure 5c,d,f,h). No primary IPGE–alloys were found. Desulphurised laurite and erlichmanite along with scarce cooperite replace primary laurite and erlichmanite, which is particularly obvious at crystal rims (Figure 5a,e,f). Pt–Cu alloys and Os–Pt–Ir alloys, as well as PPGM sulphides and/or sulpharsenides are frequently associated with IPGE–Ni alloys, desulphurised irarsite and irarsite-platarsite, but also show overgrowths at the rims of primary PGM (Figure 5a,b,e,g). Desulphurised irarsite, irarsite-osarsite and rarely cooperite replace primary irarsite. Secondary PGM assemblages in both the fine tip and chromite fractions from Tsangli are less abundant. Apart from the abovementioned merenskyite, the PGM include mainly irarsite, ruarsite-osarsite, scarce sulpharsenides and IPGE–Ni alloys after primary laurite and erlichmanite (Figures 6c,d and 7). Other desulphurised phases were not observed in Tsangli.

## 6. Discussion

### 6.1. Advantages to the PGM Study from Their Beneficiation

The current study provides new data on the PGM occurrence and assemblage from the Othrys chromitites, which are important for petrogenetic interpretations, as well as for mineral processing. Sample preparation and data collection has a strong impact on the PGM characterisation and the assessment of their bulk mineralogical composition. This has even stronger effect in the case of low-grade PGM samples, like in most of the ophiolitic chromitites. Observed PGM grains from in situ studies of the host rocks likely fail to reflect the entire variety of PGM, especially when their grain sizes are below 10  $\mu\text{m}$ . Such tiny grains, which are included in their host minerals, have much less chances to be detected and identified. On the contrary, concentrates prepared from a large amount of a homogenised material are more representative and provide a comprehensive image of the PGM assemblages. This study revealed a wider range of PGM phases and grain sizes compared to previous studies from in situ investigations in Othrys [16]. Therefore, it is recommended that fine milling and separation of different size fractions is an important factor for a better characterisation of PGM. In previous works, PGM were concentrated from chromitites using a hydroseparation technique, which is an efficient way for the preparation of concentrates [13,14]. In this study, we show that superpanning is another proficient technique for PGM concentration.

The study of polished sections usually is inadequate for the complete characterisation of PGM assemblages. Moreover, application of PGE contents should always be used with caution, as they do

not always reflect the PGM paragenesis in the host formations [27]. Previous studies of concentrates from Pindos and Vourinos chromitites reported a larger number of PGM grains, and a greater range of compositions, including some species that had not been detected from in situ observations, as well as a greater variation of their grain size relative to conventional studies in polished sections [13,14,17]. These methods enabled easier identification and classification into primary and secondary assemblages and led to different petrogenetic interpretations of the PGE mineralisation. More representative PGM parageneses have been reported in Pindos with the predominance of PPGM in some chromitites (Korydallos), which is unusual for ophiolites [14,17]. Conflicting studies in Vourinos had reported the occurrence of exclusively primary [1] or primary and secondary [28] PGM assemblages. The study of concentrates [13] clarified that both primary and secondary PGM parageneses are present. Significant differences between chromitites in Xerolivado (with the predominance of laurite and iridium) and Voidolakkos (dominated by secondary Ru–Os–Ir–Fe minerals) were also revealed. Nevertheless, it is recommended that both in situ and in-concentrates studies are equally necessary to fully describe the behaviour of PGM for petrogenetic purposes. The first method provides textural relations of the PGM with their host minerals, whereas the second is very important to reveal the whole PGM mineralogical range.

The investigation of the different concentrate fractions revealed the potential metallurgical importance of the current work. The PGM grains which are larger than 10–15  $\mu\text{m}$ , tend to liberate better from their host chromite host. This is inferred from the fact that grains coarser than 15  $\mu\text{m}$  were not observed in the chromite fractions (Figure 4). This observation indicates that the larger PGM grains can be liberated more effectively whereas further grinding may be required for the liberation of PGM grains smaller than 15  $\mu\text{m}$ .

## 6.2. Petrogenetic Implications

Significant differences in the amount of PGM and the bulk PGM mineralogy between the samples from west and east Othrys were revealed, which were very difficult to be detected via in situ observations. Restricted ore bodies of sulphides and magnetite occur at the peripheral areas of the Tsangli chromitite likely associated with serpentinising fluids [29]. However, sampling of the investigated chromitites took place away from these ores, and hence any association of the PGM grains with them is precluded. The overwhelming preponderance of PGM and the greater mineralogical variability in the west Othrys (Agios Stefanos) relative to the east Othrys (Tsangli) strongly suggest that different processes may account for the petrogenesis and evolution of PGM in the two areas. A detailed investigation of the petrogenetic evolution of the two areas is dealt elsewhere (manuscript in progress) and will include whole-rock PGE data, electron microprobe data of the PGM and spinels. However, the current observed differences can be attributed to different degrees of partial melting and melt impregnation of the mantle in the two areas, suggesting the occurrence of a large mantle inhomogeneity. This interpretation is consistent with previous works, which have shown that the west Othrys ophiolite is related with an extension regime (back-arc basin or MORB; [23,24,30]), while the east Othrys ophiolite is strongly associated with a supra-subduction zone setting (SSZ; [24,31]).

The predominance of primary laurite and erlichmanite, and the exclusive appearance of sperrylite in Tsangli are in accordance with findings from in situ observations from Garuti et al. [16]. However, the current data suggest that erlichmanite and laurite-erlichmanite extensive solid solutions are common and relatively more abundant in the west Othrys. We suggest that underestimation of the participation of erlichmanite from in situ observations is related to the much larger grain size of laurite, a fact that may lead to biased results.

Unlike most ophiolitic chromitites (e.g., [4,32–34]), including the well-known Pindos and Vourinos complexes in Greece [1,13–15,17,18,28,35–37], primary alloys of the IPGE subgroup were not found in Agios Stefanos. This is similar to Skyros and Rhodope complexes [38,39] strongly indicating that  $f_{\text{S}_2}$  was sufficiently high from the beginning of the magmatic evolution of the west Othrys chromitites. Most likely,  $f_{\text{S}_2}$  was raised above the Os–Os<sub>2</sub> buffer, as it is deduced by the appearance of erlichmanite.

Local fluctuations of the  $f_{As}$ , which may be related to influx of melts or fluids in an open system, can explain the formation of irarsite-osarsite grains. On the contrary, the existence of primary Os–Ir (and Ru-poor, Ni-free) inclusions in PGM from Tsangli indicates an initial (and perhaps short-lived) percolation of S-undersaturated melts, consistent with the SSZ origin of the east Othrys ophiolite. This episode was followed by an influx of melts or fluids in an open system and a rapid increase of  $f_{S_2}$  that destabilised the alloys and promoted the precipitation of IPGE-sulphides, similar to Agios Stefanos.

The occurrence of primary sperrylite only in Tsangli, is another strong contrast between the west and east Othrys complexes. Pt and Pd minerals are commonly located at the Moho transition zone, either at the uppermost mantle or in the lower cumulates [27], as melts derived from high degrees of partial melting of a fertile mantle ascend, differentiate and impregnate the uppermost mantle region [5,40]. Therefore, it is concluded that the east Othrys ophiolite was located close to the Moho transition zone, at a higher level relative to the west Othrys.

PGM are susceptible to alteration during serpentinisation of their host chromitites and peridotites (e.g., [28,41,42]). We interpret the desulphurised phases of laurite and erlichmanite, as well as the associated IPGE–Ni alloys, occurring in Agios Stefanos, as products of such an episode. Most likely, the primary PGM sulphides reacted with late S-undersaturated fluids, which are common in ophiolitic peridotites (e.g., [43,44]). These fluids caused a sequential decrease of  $f_{S_2}$  in the mantle source region resulting in the progressive depletion of S from the primary IPGE-sulphides. Eventually, IPGM alloys were formed where Ni, most probably delivered from the serpentinising fluids, substituted for S. Desulphurised phases were not observed in Tsangli, however the occurrence of secondary IPGE–Ni alloys likely indicate a complete desulphurisation event. Secondary PGM and sulpharsenides of the PPGE subgroup in Agios Stefanos form small discrete grains replacing mostly primary erlichmanite and irarsite. This is interpreted as the result of the infiltration of either late magmatic or post-magmatic fluids, which caused local redistribution of PPGE and deposition of PPGM with the aid of As ligands [45]. Secondary minerals of the ruarsite-osarsite-irarsite series in both areas highlight the importance of high As activity during the secondary processes.

## 7. Conclusions

Separation of PGM from two composite chromitite samples from east (Tsangli) and west (Agios Stefanos) Othrys, using superpanning, allowed the identification of a larger variety and a greater number of grains relative to conventional studies. Laurite and erlichmanite are the most abundant PGM in both regions and a more realistic ratio of their modal abundances is presented. The chromitite from Agios Stefanos shows a larger variability and a greater number of PGM grains relative to that from Tsangli. Primary irarsite occurs in Agios Stefanos, whereas primary IPGE-alloys and sperrylite occur exclusively in Tsangli. The PGM assemblages from the two regions reflect a different evolution. It is probable that the east and west Othrys ophiolites have been evolved at different mantle levels with different fluctuations of  $f_{S_2}$  and  $f_{As}$ . Secondary processes in Agios Stefanos developed a larger mineralogical variability than Tsangli with the formation of a progressive series of desulphurised phases of the primary sulphides and IPGE–Ni alloys, sulpharsenides and PPGM. Few sulpharsenides and IPGE–Ni alloys were developed in Tsangli. More detailed petrological studies, comparing concentrated and non-concentrated samples from the chromitites of Othrys could possibly unveil the missing link between the Pindos-Othrys-Vourinos geotectonic evolution.

**Acknowledgments:** The authors are grateful to two anonymous reviewers for critical comments that largely improved the manuscript.

**Author Contributions:** Basilios Tsikouras participated in the field work and in the interpretation of the results, coordinated the research and wrote the paper; Elena Ifandi participated in the interpretation of results and wrote the paper; Sofia Karipi conducted most of the field work, acquired data, performed SEM work and participated in the interpretation of results; Tassos A. Grammatikopoulos organised and prepared the concentrates and the polished samples and participated in the interpretation of results; and Konstantin Hatzipanagioutou participated in the interpretation of results.

**Conflicts of Interest:** The authors declare no conflict of interest.

## References

1. Augé, T. Platinum-group mineral inclusions in ophiolitic chromitite from the Vourinos Complex, Greece. *Can. Mineral* **1985**, *23*, 163–171.
2. Ferrario, A.; Garuti, G. Platinum-group mineral inclusions in chromitites of the Finero mafic-ultramafic complex (Ivrea-Zone, Italy). *Mineral. Petrol.* **1990**, *41*, 125–143. [[CrossRef](#)]
3. Pedersen, R.B.; Johannesen, G.M.; Boyd, R. Stratiform platinum-group element mineralizations in the ultramafic cumulates of the Leka ophiolite complex, central Norway. *Econ. Geol.* **1993**, *88*, 782–803. [[CrossRef](#)]
4. Garuti, G.; Zaccarini, F.; Moloshag, V.; Alimov, V. Platinum-group elements as indicators of sulphur fugacity in ophiolitic upper mantle: An example from chromitites of the Ray-Iz ultramafic complex, Polar Urals, Russia. *Can. Mineral.* **1999**, *37*, 1099–1115.
5. Ahmed, A.H.; Arai, S. Platinum-group minerals in podiform chromitites of the Oman ophiolite. *Can. Mineral.* **2003**, *41*, 597–616. [[CrossRef](#)]
6. Burton, K.W.; Schiano, P.; Birck, J.L.; Allègre, C.J. Osmium isotope disequilibrium between mantle minerals in a spinel-lherzolite. *Earth Planet. Sci. Lett.* **1999**, *172*, 311–322. [[CrossRef](#)]
7. Harvey, J.; Gannoun, A.; Burton, K.W.; Schiano, P.; Rogers, N.W.; Alard, O. Unravelling the effects of melt depletion and secondary infiltration on mantle Re–Os isotopes beneath the French Massif Central. *Geochim. Cosmochim. Acta* **2010**, *74*, 293–320. [[CrossRef](#)]
8. González-Jiménez, J.M.; Griffin, W.L.; Gervilla, F.; Proenza, J.A.; O'Reilly, S.Y.; Pearson, N.J. Chromitites in ophiolites: How, where, when, why? Part I. A review and new ideas on the origin and significance of platinum-group minerals. *Lithos* **2014**, *189*, 127–139. [[CrossRef](#)]
9. Naldrett, A.J.; Hoffman, E.L.; Green, A.H.; Chou, C.L.; Naldrett, S.R.; Alcock, R.A. The composition of Ni-sulfide ores, with particular reference to their content of PGE and Au. *Can. Mineral.* **1979**, *17*, 403–415.
10. Garuti, G.; Fershtater, G.; Bea, F.; Montero, P.; Pushkarev, E.V.; Zaccarini, F. Platinum-group elements as petrological indicators in mafic-ultramafic complexes of the central and southern Urals: Preliminary results. *Tectonophysics* **1997**, *276*, 181–194. [[CrossRef](#)]
11. Walker, R.J. Highly siderophile elements in the Earth, Moon and Mars: Update and implications for planetary accretion and differentiation. *Chem. Erde Geochem.* **2009**, *69*, 101–125. [[CrossRef](#)]
12. O'Driscoll, B.; González-Jiménez, J.M. Petrogenesis of the platinum-group minerals. *Rev. Mineral. Geochem.* **2016**, *81*, 489–578. [[CrossRef](#)]
13. Kapsiotis, A.; Grammatikopoulos, T.; Zaccarini, F.; Tsikouras, B.; Garuti, G.; Hatzipanagiotou, K. PGM characterization in concentrates from low grade PGE chromitites from the Vourinos ophiolite complex, northern Greece. *Appl. Earth Sci.* **2006**, *115*, 49–57. [[CrossRef](#)]
14. Grammatikopoulos, T.; Kapsiotis, A.; Zaccarini, F.; Tsikouras, B.; Hatzipanagiotou, K.; Garuti, G. Investigation of platinum-group minerals (PGM) from Pindos chromitites (Greece) using hydroseparation concentrates. *Miner. Eng.* **2007**, *20*, 1170–1178. [[CrossRef](#)]
15. Kapsiotis, A.; Grammatikopoulos, T.A.; Tsikouras, B.; Hatzipanagiotou, K.; Zaccarini, F.; Garuti, G. Chromian spinel composition and platinum-group element mineralogy of the chromitites from Milia area, Pindos ophiolite complex, Greece. *Can. Mineral.* **2009**, *47*, 1037–1056. [[CrossRef](#)]
16. Garuti, G.; Zaccarini, F.; Economou-Eliopoulos, M. Paragenesis and composition of laurite from chromitites of Othrys (Greece): Implications for Os–Ru fractionation in ophiolite upper mantle of the Balkan peninsula. *Miner. Depos.* **1999**, *34*, 312–319. [[CrossRef](#)]
17. Kapsiotis, A.; Grammatikopoulos, T.A.; Tsikouras, B.; Hatzipanagiotou, K. Platinum-group mineral characterization in concentrates from high-grade PGE Al-rich chromitites of Korydallos area in the Pindos ophiolite complex (NW Greece). *Resour. Geol.* **2010**, *60*, 178–191. [[CrossRef](#)]
18. Kapsiotis, A.; Grammatikopoulos, T.A.; Tsikouras, B.; Hatzipanagiotou, K.; Zaccarini, F.; Garuti, G. Mineralogy, composition and PGM of chromitites from Pefki, Pindos ophiolite complex (NW Greece): Evidence for progressively elevated fAs conditions in the upper mantle sequence. *Mineral. Petrol.* **2011**, *101*, 129–150. [[CrossRef](#)]
19. Kocks, H.; Melcher, F.; Meisel, T.; Burgath, K.P. Diverse contributing sources to chromitite petrogenesis in the Shebenik Ophiolitic Complex, Albania: Evidence from new PGE- and Os-isotope data. *Mineral. Petrol.* **2007**, *91*, 139–170. [[CrossRef](#)]

20. Smith, A.G.; Hynes, A.J.; Menzies, M.; Nisbet, E.G.; Price, I.; Welland, M.J.; Ferrière, J. The stratigraphy of the Othris Mountains, eastern central Greece: A deformed Mesozoic continental margin sequence. *Ecol. Geol. Helv.* **1975**, *68*, 463–481.
21. Smith, A.G. Tectonic significance of the Hellenic-Dinaric ophiolites. In *Magmatic Processes and Plate Tectonics*; Prichard, H.M., Alabaster, T., Harris, N.B.W., Neary, C.R., Eds.; Geological Society Special Publication: London, UK, 1993; Volume 76, pp. 213–243.
22. Dijkstra, A.H.; Drury, M.R.; Vissers, R.L.M. Structural petrology of plagioclase peridotites in the West Othrys Mountains (Greece): Melt impregnation in mantle lithosphere. *J. Petrol.* **2001**, *42*, 5–24. [[CrossRef](#)]
23. Barth, M.G.; Mason, P.R.D.; Davies, G.R.; Dijkstra, A.H.; Drury, M.R. Geochemistry of the Othris ophiolite, Greece: Evidence for refertilization? *J. Petrol.* **2003**, *44*, 1759–1785. [[CrossRef](#)]
24. Barth, M.G.; Gluhak, T.M. Geochemistry and tectonic setting of mafic rocks from the Othris ophiolite, Greece. *Contrib. Mineral. Petrol.* **2009**, *157*, 23–40. [[CrossRef](#)]
25. Tsikouras, B.; Karipi, S.; Rigopoulos, I.; Perraki, M.; Pomonis, P.; Hatzipanagiotou, K. Geochemical processes and petrogenetic evolution of rodingite dykes in the ophiolite complex of Othrys (Central Greece). *Lithos* **2009**, *113*, 540–554. [[CrossRef](#)]
26. Rigopoulos, I.; Tsikouras, B.; Pomonis, P.; Hatzipanagiotou, K. Determination of the interrelations between the engineering parameters of construction aggregates from ophiolite complexes of Greece using factor analysis. *Constr. Build. Mater.* **2013**, *49*, 747–757. [[CrossRef](#)]
27. Malitch, K.N.; Thalhammer, O.A.; Knauf, V.V.; Melcher, F. Diversity of platinum-group mineral assemblages in banded and podiform chromitite from the Kraubath ultramafic massif, Austria: Evidence for an ophiolitic transition zone? *Miner. Deposita* **2003**, *38*, 282–297.
28. Garuti, G.; Zaccarini, F. In situ alteration of platinum-group minerals at low temperature: Evidence from serpentinized and weathered chromitite of the Vourinos complex, Greece. *Can. Mineral.* **1997**, *35*, 611–626.
29. Economou, M.I.; Naldrett, A.J. Sulfides associated with podiform bodies of chromite at Tsangli, Eretria, Greece. *Miner. Depos.* **1984**, *419*, 289–297. [[CrossRef](#)]
30. Dijkstra, A.H.; Barth, M.G.; Drury, M.R.; Mason, P.R.D.; Vissers, R.L.M. Diffuse porous melt flow and melt-rock reaction in the mantle lithosphere at a slow-spreading ridge: A structural petrology and LA-ICP-MS study of the Othris Peridotite Massif (Greece). *Geochem. Geophys. Geosyst.* **2003**, *4*, 8613. [[CrossRef](#)]
31. Magganas, A.; Koutsovitis, P. Composition, melting and evolution of the upper mantle beneath the Jurassic Pindos ocean inferred by ophiolitic ultramafic rocks in East Othris, Greece. *Int. J. Earth Sci.* **2015**, *104*, 1185–1207. [[CrossRef](#)]
32. Brenan, J.M.; Andrews, D. High-temperature stability of laurite and Ru–Os–Ir alloy and their role in PGE fractionation in mafic magmas. *Can. Mineral.* **2001**, *39*, 341–360. [[CrossRef](#)]
33. Andrews, D.R.A.; Brenan, J.M. Phase-equilibrium constraints on the magmatic origin of laurite + Ru–Os–Ir alloy. *Can. Mineral.* **2002**, *40*, 1705–1716. [[CrossRef](#)]
34. González-Jiménez, J.M.; Griffin, W.L.; Proenza, J.A.; Gervilla, F.; O'Reilly, S.Y.; Akbulut, M.; Pearson, N.J.; Arai, S. Chromitites in ophiolites: How, where, when, why? Part II. The crystallisation of chromitites. *Lithos* **2014**, *189*, 140–158. [[CrossRef](#)]
35. Grammatikopoulos, T.A.; Kapsiotis, A.; Tsikouras, B.; Hatzipanagiotou, K.; Zaccarini, F.; Garuti, G. Spinel composition, PGE geochemistry and mineralogy of the chromitites from the Vourinos ophiolite complex, northwestern Greece. *Can. Mineral.* **2011**, *49*, 1571–1598. [[CrossRef](#)]
36. Tarkian, M.; Economou-Eliopoulos, M.; Sambanis, G. Platinum-group minerals in chromitites from the Pindos ophiolite complex, Greece. *Neues Jahrb. Mineral. Monatshefte* **1996**, *4*, 145–160.
37. Prichard, H.M.; Economou-Eliopoulos, M.; Fisher, P.C. Contrasting platinum-group mineral assemblages from two different podiform chromitite localities in the Pindos ophiolite complex, Greece. *Can. Mineral.* **2008**, *46*, 329–341. [[CrossRef](#)]
38. Tarkian, M.; Naidenova, E.; Zhelyaskova-Panayotova, M. Platinum-group minerals in chromitites from the Eastern Rhodope ultramafic complex, Bulgaria. *Mineral. Petrol.* **1991**, *44*, 73–87. [[CrossRef](#)]
39. Tarkian, M.; Economou-Eliopoulos, M.; Eliopoulos, D.G. Platinum-group minerals and tetraauricupride in ophiolitic rocks of Skyros Island, Greece. *Mineral. Petrol.* **1992**, *47*, 55–66. [[CrossRef](#)]
40. Prichard, H.M.; Lord, R.A.; Neary, C.R. A model to explain the occurrence of platinum- and palladium-rich ophiolite complexes. *J. Geol. Soc.* **1996**, *153*, 323–328. [[CrossRef](#)]

41. Zaccarini, F.; Proenza, J.A.; Ortega-Gutiérrez, F.; Garuti, G. Platinum group minerals in ophiolitic chromitites from Tehuiztzingo (Acatlán complex, southern Mexico): Implications for post-magmatic modification. *Mineral. Petrol.* **2005**, *84*, 147–168. [[CrossRef](#)]
42. Proenza, J.A.; Zaccarini, F.; Escayola, M.; Cávana, C.; Shalamuk, A.; Garuti, G. Composition and textures of chromite and platinum-group minerals in chromitites of the western ophiolitic belt from Pampeans Ranges of Córdoba, Argentina. *Ore Geol. Rev.* **2008**, *33*, 32–48. [[CrossRef](#)]
43. Kelemen, P.B.; Dick, H.J.B.; Quick, J.E. Formation of harzburgite by pervasive melt/rock reaction in the upper mantle. *Nature* **1992**, *358*, 635–641. [[CrossRef](#)]
44. Peregoedova, A.; Barnes, S.J.; Baker, D.R. The formation of Pt–Ir alloys and Cu–Pd-rich sulfide melts by partial desulfurization of Fe–Ni–Cu sulfides: Results of experiments and implications for natural systems. *Chem. Geol.* **2004**, *208*, 247–264. [[CrossRef](#)]
45. Graham, I.T.; Franklin, B.J.; Marshall, B. Chemistry and mineralogy of podiform chromitite deposits, southern NSW, Australia: A guide to their origin and evolution. *Mineral. Petrol.* **1996**, *57*, 129–150. [[CrossRef](#)]



© 2016 by the authors; licensee MDPI, Basel, Switzerland. This article is an open access article distributed under the terms and conditions of the Creative Commons Attribution (CC-BY) license (<http://creativecommons.org/licenses/by/4.0/>).